Australian Earthquake Engineering Society
2024 National Conference, 21-23 November 2024
Adelaide, South Australia, Australia

Evaluation of the Safety of Reinforced Concrete Buildings Post-Earthquake for Swift Rescue and Recovery

Prashidha Khatiwada[1], Bipul Neupane[1], Mojtaba Akhoundi Khezrabad[1], Elisa Lumantarna[1], Nelson Lam[1]

1. Department of Infrastructure Engineering, University of Melbourne, Parkville VIC 3010

Abstract

Recent seismic events highlight the critical need for effective online tools for the rapid assessment of the safety of buildings in an earthquake affected area. This study presents an innovative rapid assessment procedure utilising a virtual city model to evaluate the post-earthquake safety of a large number of buildings in the aftermath of a major event. The aim is to support decision-making for expediting rescue and post-disaster recovery. The conventional approach to damage prediction is employing earthquake ground motion based on a hypothetical earthquake scenario (as defined by a magnitude-distance combination) along with archetype models of the affected buildings. This "scenario-based" approach to damage predictions would not give accurate assessment of damage caused by a real earthquake that has occurred because events of the same earthquake scenario can be very different. Buildings of the same archetype can also be very different. This article introduces the concept of an "event-based" ground motion model. Existing scenario-based ground motion models are combined with crowd-sourced damage reports along with site subsoil models to develop ground motion models which is specific to an earthquake event for accurate simulation of damage to buildings to assist rescue and recovery work. Structural details of the existing building stock in the earthquake affected area are typically lacking. A swift input process to reconstruct these details are necessary. To address this, geometric and structural details of buildings are rapidly obtained by utilising building footprint data and rooftop features from open datasets and remote sensing images. This approach facilitates the swift development of comprehensive macroscopic building models. Subsequently, a Rapid Nonlinear Time History Analysis (RNLTHA) engine developed by the authors based on macro modelling of the building structures is then applied to provide fast and realistic predictions without requiring long computational time. Utilisation of the RGB cameras, laser scanners, and Ground Penetrating Radar (GPR) are recommended to obtain more detailed damage assessments of selected buildings. The objective is to guide decisions on rescue operation (informing risks of collapse when subject to aftershocks), immediate reoccupation, priority with retrofitting and reconstruction. A case study based at Melbourne, featuring a publicly accessible virtual city model (available at https://quakeadvice.org), demonstrates the efficacy of the proposed methodology in the real-world contexts.

Keywords: RC buildings; virtual city, seismic assessment; event-based predictions.

1 Introduction

Seismic events often result in widespread devastation, impacting not only physical infrastructure but also communities and economies. The aftermath of an earthquake is a critical

period demanding swift action to ensure occupant safety, initiate rescue operations, and commence recovery efforts. Evaluating the structural integrity of buildings post-earthquake is essential to determine which structures are safe for reoccupation and which require evacuation or further inspection. Delayed or inaccurate assessments can have catastrophic consequences, including the risk of collapse during aftershocks and hindrance of timely rescue operations. Many structures in Australia remain at high risk due to the fact that earthquake hazards were integrated into Australian building codes only around 1995. Over 90% of buildings in Australia are not designed to withstand earthquakes (Harrison and Foliente, 2018), making them particularly vulnerable to seismic damage. Additionally, a significant portion of the building stock consists of reinforced concrete (RC) structures with walls that often have limited ductility. These low-ductility walls exhibit reduced seismic resistance and are prone to soil-structure resonance, leading to increased seismic demand and poor performance (Tsang et al., 2017). Historical events such as the 1989 Newcastle Earthquake and the 2010 Kalgoorlie Earthquake underscore the serious seismic risks faced by such structures.

While considerable research focuses on predicting the vulnerability of buildings to future seismic events (scenario-based prediction), there is a notable gap in research on the rapid assessment of buildings following an actual earthquake (event-based prediction). Event-based prediction faces unique challenges compared to scenario-based prediction. The primary challenge involves selecting and scaling bedrock accelerograms to represent the seismic excitation experienced at each site during an event. In scenario-based predictions, scaled bedrock accelerograms can be obtained by uploading a target spectrum generated from Ground Motion Prediction Equations (GMPEs), as described in Hu et al. (2023). In contrast, event-based prediction requires selecting and scaling recorded accelerograms using a target spectrum that reflects the observed damage intensity. Additionally, parameters in GMPEs—such as the wave transmission quality factor (which describes the frequency-dependent rate of amplitude attenuation along the wave path) and the Brune stress parameter (or stress drop, indicating fault slip as a fraction of ruptured surface area)—must be calibrated to match the specific earthquake's reported damages. To the authors' knowledge, there are no existing analytical methods for obtaining accelerograms that match the observed damage levels.

The second challenge is the time constraint in preparing input information, such as building exposure databases. Scenario-based predictions benefit from detailed geometric and mechanical information obtained through building surveys and database exploration, but this is often unfeasible post-earthquake due to time constraints. Scenario-based predictions are primarily used for future planning and mitigation, while event-based predictions impact immediate decision-making regarding reoccupation, retrofitting, or reconstruction of damaged buildings. Misjudgements in these decisions can have serious consequences, including risk to lives during aftershocks and significant economic impacts.

This paper introduces a novel approach to address the challenges of rapid post-earthquake assessment by employing a comprehensive methodology designed for swift evaluation of buildings. The proposed approach aims to expedite rescue and recovery efforts and support decisions on building reoccupation. It leverages a virtual city-based methodology, allowing for efficient identification of vulnerable buildings on a city scale. The procedure begins by sourcing and scaling event-based accelerograms using an adjusted target spectrum, based on GMPEs calibrated and optimised to reflect event-specific damages reported in crowd-sourced damage data and recorded accelerograms from the event. These accelerograms are then converted to soil surface accelerograms. Building geometries and structural details are extracted from open-source building footprint datasets and remote sensing images. This facilitated the creation of macroscopic structural models in the absence of detailed architectural plans. The Rapid Nonlinear Time History Analysis (RNLTHA) is then employed to predict building damage states with minimal computational resources. While (RNLTHA) provides critical information for assessing the safety of reoccupying a building and identifying required repairs or retrofitting, in some cases, it may present contradicting results such as damage level in between safe or unsafe for reoccupation and between reparable or non-repairable damage, requiring additional verification. For such buildings, utilisation of advanced techniques such as RGB cameras, laser scanners, and Ground Penetrating Radar (GPR) are recommended to validate and confirm

damage assessments, supporting informed decision-making regarding reoccupation, retrofitting, or reconstruction. A case study conducted in Melbourne demonstrates the efficacy of the proposed virtual city approach and its potential for improving post-earthquake damage assessments.

2 Methodologies

A virtual city-based methodology is proposed to enable rapid and accurate seismic assessment of buildings post-earthquake. This approach leverages a virtual city to efficiently identify vulnerable buildings at a city scale, assessing each building individually rather than using a typological approach. The methodology involves four key steps: first, adjusting or scaling recorded accelerograms for event-specific seismic excitations using crowd-sourced damage reports. These scaled accelerograms are then converted to soil surface accelerograms. Second, open-source building footprint dataset and remote sensing images are used to extract geometric parameters and structural details necessary for creating a macroscopic model of the building. Third, the soil surface accelerograms, and dynamic and nonlinear properties of the model are input into Rapid Nonlinear Time History Analysis (RNLTHA) to predict damage states. Lastly, RGB cameras, laser scanners, and GPR are utilised in special cases where additional verification of damage assessments is required. These advanced tools help ensure the accuracy of damage evaluations and support informed decision-making regarding building safety. Detailed explanations of these methodologies are provided in Sections 2.1 to 2.4.

2.1 Generating Earthquake Excitation for Event-Based Earthquakes

Accurate assessment of earthquake impact on a building necessitates a realistic representation of the seismic excitations experienced during the event. The proposed methodology highlights the importance of using event-specific earthquake data instead of relying solely on generic predictions. Recorded accelerograms are adjusted/scaled according to observed site damage intensity, which is gathered from crowd-sourced internet felt reports and the Community Internet Intensity (CII), which can be converted into the Modified Mercalli Intensity (MMI) scale (Wald et al., 1999). The MMI is a more meaningful measure of ground shaking severity compared to earthquake magnitude. According to Pejic & Allen (2024), MMI derived from felt reports alone can estimate potential community impact.

The process for adjusting/scaling recorded accelerograms based on observed site damage intensity is outlined as follows:

Step 1: Calculate the equivalent MMI for each felt report using Equation (1). Plot these results on a gridded map according to the locations of the felt reports. In Equation (1), CWS represents the Community Weighted Sum, derived from the questionnaire responses of individual felt reports. For details on the questionnaire and the determination of CWS, refer to Wald et al. (1999).

$$\mathrm{MMI} \cong 3.4 \log_e(\mathrm{CWS}) - 4.38 \quad (1)$$

Step 2: Calculate the mean MMI for area within the virtual city that does not feature site with deep/soft soil sediments and sparsely populated areas.

Step 3: Convert the mean MMI to the equivalent peak ground velocity (PGA_{MMI}) on bedrock (Sabegh et al., 2021; and Atkinson & Kaka, 2007). In Equation (2), the soil amplification factor (S_a) is calculated following the method proposed by Kokusho and Sato (2008) based on the ratio of the shear wave velocity of rock to the near-surface shear wave velocity of the site (upper 30 m depth). The shear wave velocity of rock is a default parameter for a precinct or an entire city affected by the earthquake, whereas the average near-surface shear wave velocity of a soil site is determined by analysis of the soil-column model as described later in this section.

$$PGV_{MMI} = \frac{10^{\frac{MMI-3.311}{3.373}}}{S_a} = \frac{10^{\frac{MMI-3.311}{3.373}}}{0.175 + 0.685\frac{V_{s,rock}}{V_{s,site}}} \quad (2)$$

Step 4: To calibrate the wave transmission quality factor 'Q_o', apply the Spectral Ratio Method (Wilkie and Gibson, 1995) using 'PGV_{MMI}' values obtained from two or more colinear locations along the wave propagation path, as shown in Equation 3. In this equation, the propagation velocity is set as '$u = V_{s,100m} = 1.5\ km/s$' (Tang et al., 2019). The frequency 'f' is determined from frequency domain analysis of the seismometer record. '$PGV(MMI)_{R_1}$' and '$PGV(MMI)_{R_2}$' represent the '$PGV(MMI)$' at distance 'R_1' and 'R_2' from the source, respectively. Typical value of 'Q_o' lies in the range of 90-900.

$$Q_o = \frac{\pi}{u} f^{0.15}(R_2 - R_1) log_e \left(\frac{R_2 * PGV(MMI)_{R_2}}{R_1 * PGV(MMI)_{R_1}}\right) \quad (3)$$

Step 5: For a range of values of the Brune stress parameter or stress drop 'σ_d' (typical range of 30 to 300 bars), use the magnitude-distance combination of the event, the calibrated 'Q_o' value from Step 4, and the kappa 'k_o' sourced from the literature (which needs to be fixed to avoid simultaneous calibration of 'σ_d' and 'k_o'), to determine the PGV at each stress drop. Next, determine the optimised 'σ_d'corresponding to the 'PGV_{MMI}' determined in Step 3.

Step 6: Use the earthquake event's magnitude and distance combination, along with the calibrated CAM parameters from Steps 4 and 5, to generate the target spectrum. To enhance the robustness of the target spectrum, calculate the mean target spectrum by averaging multiple spectra, such as the CAM spectrum along with those provided by Allen (2012), Boatwright et al. (2006), and others.

Step 7: Finally, the target spectrum is uploaded into the PEER database to source and scale relevant bedrock accelerograms. If the database does not have the accelerogram for the considered event, the accelerogram record of the event is scaled and compiled into the accelerogram ensemble to be used in the seismic assessment.

Bedrock accelerogram ensemble that have been adjusted/scaled are to be transformed into the soil surface, accounting for amplification of the seismic waves through the soil layers by site response analyses. This process requires soil column models of the building site, showing soil depth and variation of the Standard Penetration Test (SPT) data down the borehole. For large-scale seismic assessments, such as for an entire city, a comprehensive soil model is essential. Two common approaches for develop this model are the detailed borehole approach and the simplified approach. The detailed approach, which involves sourcing borehole data for each building site, is accurate but costly, time-consuming, and computationally intensive, making it impractical for large-scale modelling. In contrast, the simplified approach employs only a few representative boreholes from publicly available database to create a generalised soil model. While more cost-effective, this approach to modelling can result in inaccuracies in seismic risk assessments, particularly if the selected boreholes do not represent all the building sites accurately in large scale (city wide) evaluatios.

To address these limitations, a new approach is outlined in below (and illustrated with a case study in Section 3):

Step 1: Generate a small block or precinct-level soil map of the city using past geotechnical maps. The NEHRP site classification map, available for many cities, can be used as a the starting point.

Step 2: Compile publicly available borehole records and their locations to develop a large database of soil column models, including soil depth and SPT-N (shear wave velocity) profiles of each soil column.

Step 3: Calculate the near surface (<30 m) average shear wave velocity and site period for each borehole (see Hu et al., 2023 for calculation details) and classify them into soil classes

or ground types. Existing code classification with additional sub-classifications may be used to refine the site period bands.

Step 4: Refine the soil block map from Step 1 using GPS location data and site classifications as inferred from analyses of the individual borehole records.

Step 5: For each refined soil block, select five to ten soil columns (borehole depth vs SPT-N profile) and perform site amplification analysis to transform bedrock accelerograms into soil surface accelerograms.

Step 6: For each building within the block, repeat Rapid Nonlinear Time History Analyses using soil surface accelerograms, resulting in maximum and mean damage predictions of individual buildings across the damage affected area which can be an entire city.

A case study demonstrating this method is presented in Section 3.

2.2 Extraction of Exposure Database

Accurate and rapid extraction of building exposure data, such as spatial information, geometric details, structural elements, and mechanical properties, is crucial for robust seismic assessment of a virtual city post-earthquake. Previous studies by Lee & Kim (2013), Gavankar & Ghosh (2018), Abdollahi (2020), and Aryal & Neupane (2023) have successfully employed deep learning techniques to derive building GPS locations, footprints, and height data from publicly available maps such as OpenStreetMap (OSM) and Azure Maps. A significant challenge lies in locating lateral load-resisting structural elements, such as structural walls, within the building footprint to create accurate floor plans, which are essential for structural modeling and seismic assessment. Understanding the geometric and mechanical details of these structural walls is vital to accurately assess the building's seismic resistance.

This paper utilises open building footprint datasets and satellite images with the help of QGIS (QGIS, 2024) to extract structural details of the buildings, including the position, shape, and size of structural walls used for lift shafts and stairs. In particular, 2020 Building Footprints dataset from the City of Melbourne (City of Melbourne, 2020) was used to collect the building footprints and elevated roof geometries. Features on the roof, such as stair cupolas, lift shaft machine rooms, mechanical ventilation devices, and pressurisation units. These features are required to be installed atop structural core walls and stairs, as mandated by AS1668.1, IBC-2021, and ASHRAE-2023 for ventilation, air-conditioning, and fire and smoke control purposes. Examples of these features are illustrated in Figure 1. The positioning, shape, size, and aspect ratio of these features within the building footprint provide preliminary insights into the possible geometric details of the structural walls. These can then be correlated with design practices to deduce the structural walls' geometrical details. For instance, according to Menegon et al. (2018), typical shapes of structural walls in Australian elevator shafts and stairs include single and double C-shaped, T-shaped, U-shaped, and core walls, as shown in Figure 2.

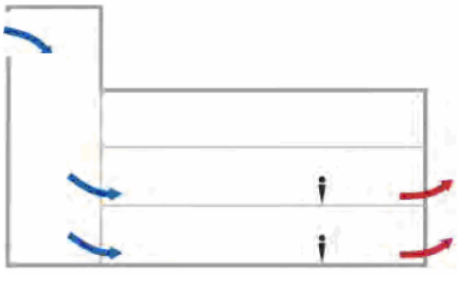

(a) Naturally ventillated stair cupola (Bhatia, 2013)

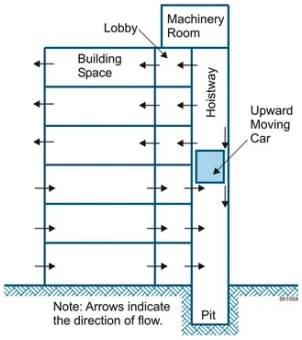

(b) Lift shaft with machine room (Hurley et al., 2015)

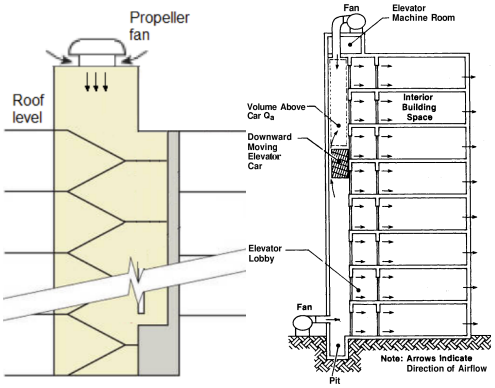

(c) Stairs and lift shaft with mechinical ventillation (Bhatia, 2013 and Kolte, 1988)

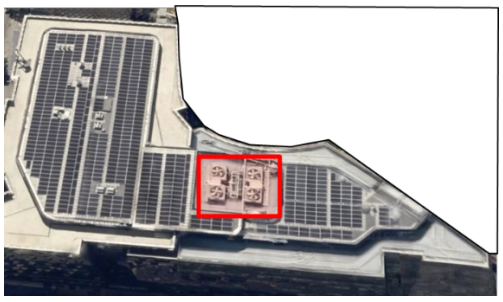

(d) Lift shaft with pressurisation units

Figure 1. Typical staircase and lift core features at the roof level of the building.

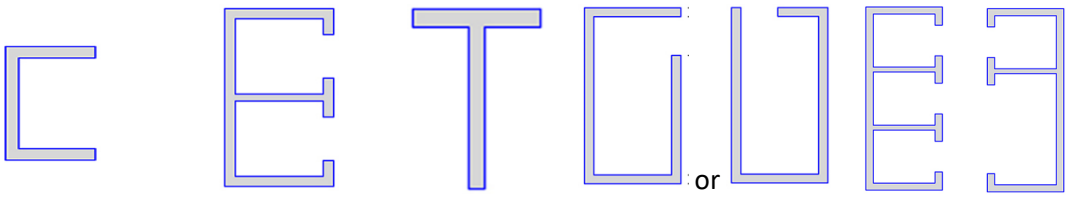

(a) C-shaped 1 (b) C-shaped 2 (c) T-shaped (d) U-shaped stairs (e) Core wall

Figure 2. Typical shapes of structural walls used in Australian lift core and stairs.

It is proposed to use high-resolution aerial images from facilities such as Nearmap (Nearmap, 2024) as the basemap for extracting roof features. The extracted features may then be validated using platforms like Google Earth (Google Earth, 2024), which provides high-resolution satellite imagery. The following rules are employed for feature detection:

Rule 1: Elevated structures detection

Identify elevated stair cupolas and lift shaft machine rooms by detecting footprints (smaller than building footprint/roofprint) of features with an footprint areas between 5 and 100 square meters.

Rule 2: Mechanical ventilation units detection

Detect mechanical ventilation units by identifying cylindrical or round propeller fans with a prominent blade assembly, connected to visible ducts. These units are often characterised by their open or grille-covered design.

Rule 3: Pressurisation units detection

Identify pressurisation units by locating roof-mounted fans with a more substantial, enclosed design intended to handle high-pressure air. These fans are typically not connected to ducts, distinguishing them from mechanical ventilation units.

Rule 4: Proximity exclusion

Exclude mechanical ventilation and pressurisation units that are either enclosed by or located in close proximity to elevated structures, such as stair cupolas and lift shaft machine rooms, to avoid counting redundant features.

Rule 5: Area limitation

Limit the total gross footprint area of these features to a maximum of 15% of the building's footprint area (as observed in the case study). If the total area exceeds this threshold, remove features that least match the criteria to ensure accurate representation.

Once the location, shape, and size of the structural core walls and stairs are identified, the reinforcement content can be determined by redesigning the building according to the seismic standards applicable at the time of its original construction. The relevant codes can be traced based on the construction year, and mechanical properties such as concrete and reinforcement strength grades can be estimated using historical trends, as demonstrated by Khatiwada et al. (2023a). The seismic floor loads and the design axial loads (N*) for the walls can be calculated by multiplying the seismic mass density by the building's volume (footprint area × height) and the axial load density by the tributary volume (tributary area × height), respectively. A parametric study conducted on 59 buildings in Melbourne was undertaken to determine typical building mass density and axial load (N^*) values, considering different live load ratings (LLR), which reflect varying building functionalities. The results, presented in Figure 3, show the building density and axial load for different live load ratings, leading to the development of closed-form expressions, as shown in Equations (4) and (5), based on curve fitting of the results. To further address the challenges posed by input uncertainties, which can significantly impact the accuracy of seismic assessments, this study adopts Monte Carlo Simulation (MCS). This method allows for variations in input parameters such as wall length and thickness, material strengths, and reinforcement content, enabling the prediction of maximum and mean damages.

$$\text{Seismic mass (tonnes)} = (0.0088 * LLR + 0.2) * \text{footprint area} * \text{height} \quad (4)$$

$$N^*(\text{kN}) = (0.4316 * LLR + 2.37) * \text{tributary area} * \text{height} \quad (5)$$

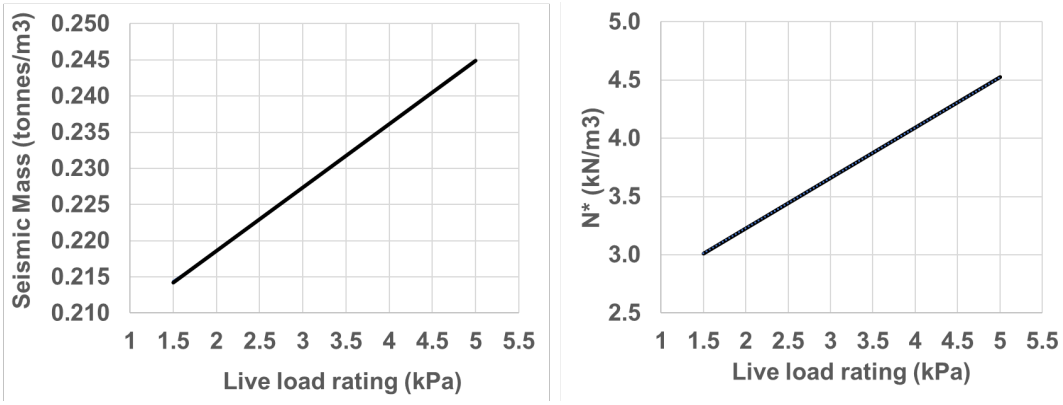

(a) Seismic mass density (b) Axial load density

Figure 3. Results of the seismic mass density and axial load density obtained from the parametric study of 59 buildings in Melbourne.

By automating the extraction of the exposure database, this approach effectively addresses the challenges of limited time and resources available in the aftermath of an earthquake. The extracted data forms the foundation for creating macroscopic structural models of buildings

within the virtual city environment. The execution of rapid dynamic analysis on these macroscopic models and the prediction of building damage levels are detailed in Section 2.3.

2.3 Damage Prediction Using Rapid Nonlinear Time History Analysis

The seismic vulnerability of a building is expressed in terms of damage states, which are defined based on the building's responses to an earthquake, such as seismic drift and material strains. To determine these seismic responses for each building in the virtual city, each structure is represented by a macroscopic model, and Rapid Nonlinear Time History Analysis (RNLTHA) is performed. The details of the macroscopic model and the RNLTHA procedure, along with validation across a wide range of RC buildings, are presented in Khatiwada et al. (2023b). The earthquake excitation input for the RNLTHA includes soil surface accelerograms, as described in Section 2.1, and the trilinear nonlinear pushover curve derived from Khatiwada et al. (2023c) using the structural wall details from Section 2.2. The simplified trilinear pushover curve, which requires only basic input information, is adopted here instead of a more detailed nonlinear fibre section analysis, as only limited building information can be extracted from the remote sensing images. By employing RNLTHA, which utilises only four degrees of freedom (DOFs) per building, computation time is reduced by approximately 95% compared to conventional Finite Element Analysis.

Damage states are determined by evaluating roof drift (calculated as the roof displacement divided by the building height) and the strain magnitudes in concrete and steel, as reported by the RNLTHA. Based on five thresholds for drift and strain, six damage states are defined: no damage, slight damage, moderate damage, extensive damage (life safety), complete damage, and collapse. Generally, buildings with damage up to slight damage can be safely reoccupied, moderate damage can be re-occupied after repairs, while those with extensive damage require retrofitting. Complete damage may necessitate significant retrofitting, but from an economic standpoint, reconstruction might be more feasible. A collapse state indicates the need for complete building reconstruction. For further details on the correlation between seismic responses and damage states, as well as descriptions of each damage state, refer to Khatiwada et al. (2023a).

2.4 Damage Confirmation Using RGB Cameras, Laser Scanners and GPR

While Rapid Nonlinear Time History Analysis (RNLTHA) provides critical information for assessing the safety of reoccupying a building and identifying required repairs or retrofitting, there are specific scenarios where additional confirmation is needed. RNLTHA might indicate that a building is either safe or unsafe for reoccupation based on predicted damage levels, but in some cases, it may present results that fall in between these extremes. For instance, if RNLTHA suggests that the building is borderline safe or unsafe for reoccupation, or if the analysis indicates that the damage might be reparable but could also be extensive, additional verification is essential. In such situations, RGB cameras, laser scanners, and GPR are employed to provide a more detailed assessment.

RGB cameras are cheap and widely available devices that acquire data from visible objects in the form of images. CNN networks trained on images enable the detection of visible damage, categorising them, and conducting spatial measurements on them. Laxman et al. (2023) used a two-step process using images and CNN to detect cracks in concrete and estimate their depth. Zou et al. (2022) used a modified version of YOLOv4 to detect multicategory damages based on post-earthquake images, facilitating safety assessment for RC structures.

RGB cameras are passive sensors sensitive to illuminating conditions. Laser scanners can fill this gap and offer more geometric accuracy. They sample the geometry of objects as dense groups of points with their precise 3D coordinates. In addition to detecting cracks, laser scanners enable modelling of damaged elements. Lou et al. (2024) used NL-3DCrack model

for semantic segmentation of crack points collected by laser scanners. Guo et al. (2023) used a smartphone's laser scanner point clouds to detect concrete spalling damage in RC shear walls and further evaluate these damages' effects on the wall's seismic performance. Shu et al. (2023) applied a slice-based approach to model damaged RC beams from point clouds.

Applications of laser scanners and RGB images are limited to inspection of visible damage. This can be covered by GPR, a non-destructive geophysical method using radar pulses to image the subsurface. Utilising this technology, rebars' position and dimensions, cracks in concrete, and deterioration can be detected. Tong et al. (2017) used a CNN network capable of detecting concealed cracks, measuring their length, and 3D reconstruction of them. Hasan & Yazdani (2016) used a regression model with normalised signal amplitude as input to predict rebars' diameter.

These mentioned technologies help verify the extent of the damage, ensuring that a building assessed as potentially safe or reparable by RNLTHA is indeed in a condition that justifies reoccupation or repair. This thorough evaluation is crucial for making informed decisions about retrofitting or reconstruction and ensuring the safety of rescue personnel and future occupants.

3 Case Study Analysis

The CLUE area of Melbourne (City of Melbourne, 2020) was selected as a case study to demonstrate the effectiveness of the proposed methodologies. Twenty low- to mid-rise reinforced concrete buildings (ranging from 2 to 11 storeys) within the CLUE area were chosen to (1) validate the proposed methodologies and (2) demonstrate the application of the virtual city in a post-earthquake context. To validate the automatic extraction of building footprints and structural wall details (as outlined in Section 2.2), high-resolution aerial images from Nearmap were used as the basemap for extracting roof features. Figure 4 presents an example comparing building dimensions (length and width) and structural wall details extracted from feature detection with the actual floor plans of the buildings, showing a close match. After predicting the shape, size, and position of the structural walls, the relevant Australian codes used for the design of each building were identified based on construction year data, and the reinforcement content in the walls was determined by redesigning the buildings according to these standards. Finally, Figure 5 compares the trilinear force-displacement capacity curve (pushover curve) derived from the extracted data, labeled as 'predicted' (red dashed line), with the actual data from the real floor plans, labeled as 'original' (blue line). The close match in this comparison confirms the robustness of the proposed method.

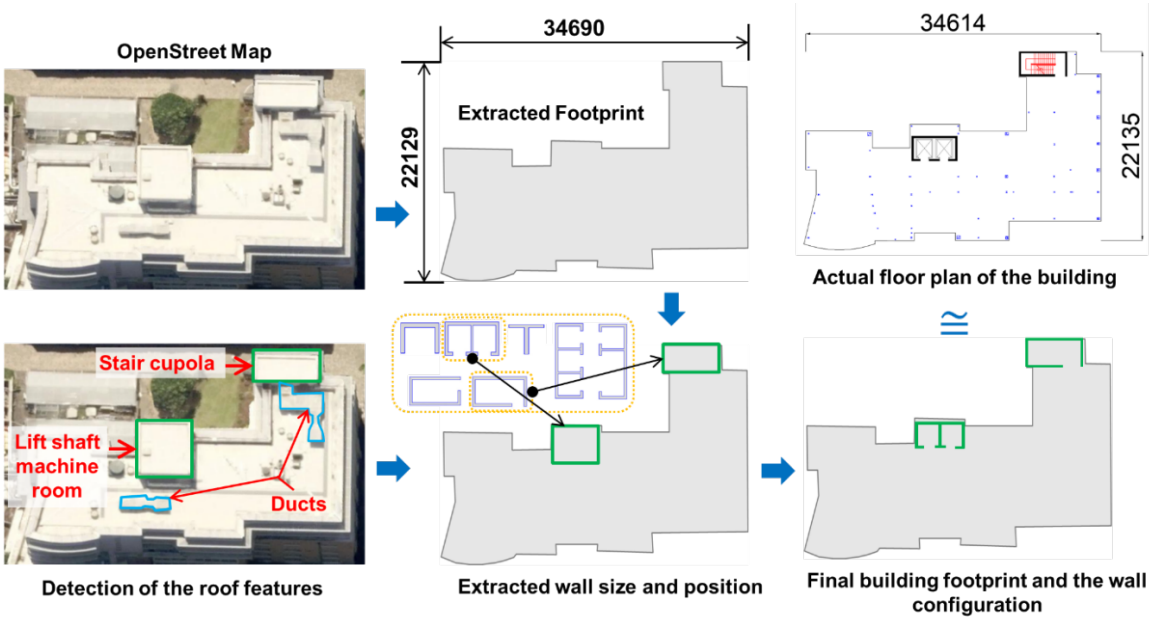

Figure 4. Example of the extraction of the floor plan and structural details from one of the case study buildings.

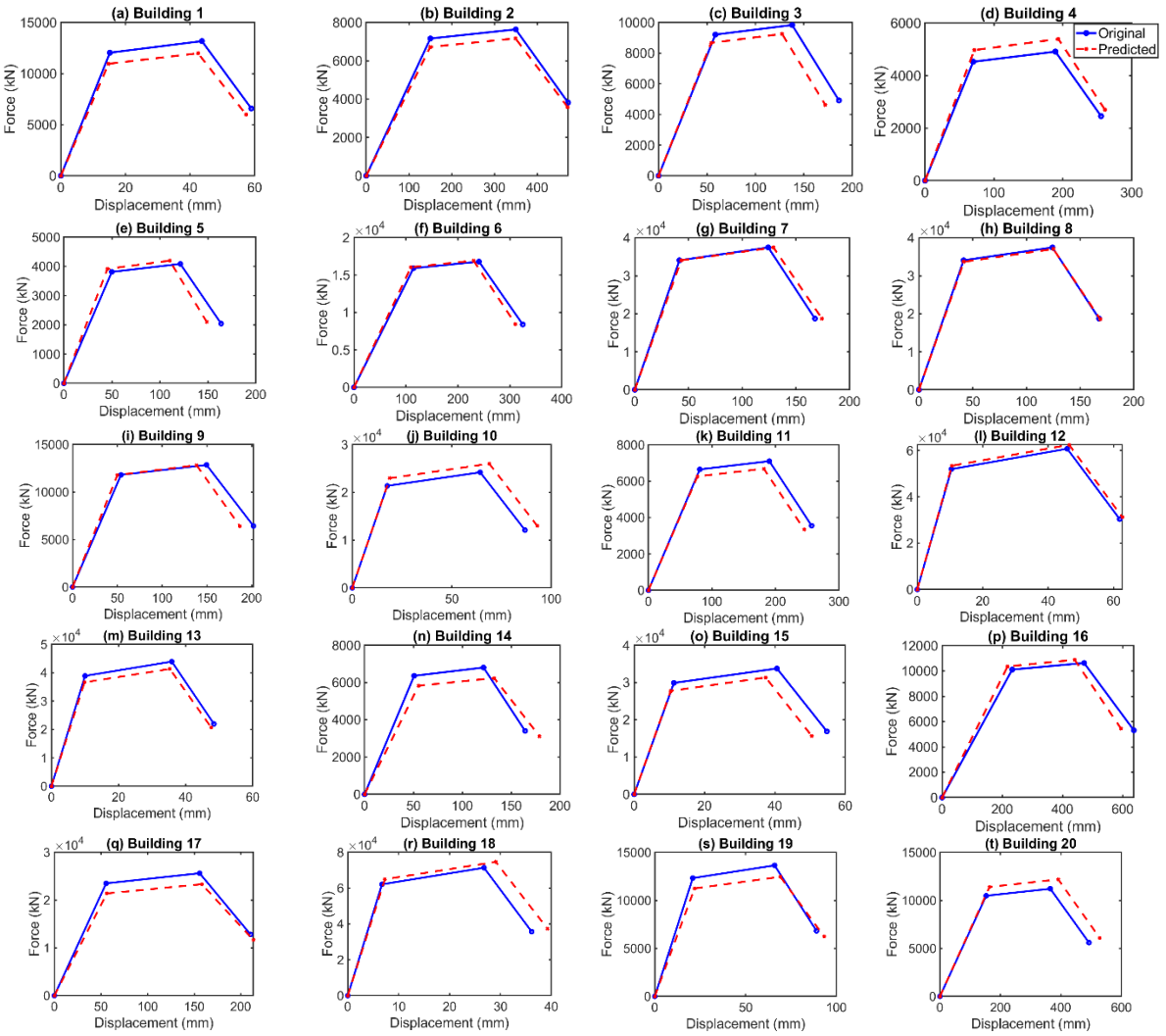

Figure 5. Comparison of the trilinear force displacement capacity curve of the case study building obtained from structural details of the building generated from the proposed method (predicted) vs the actual floor plan (original).

The 2021 Woods Point, Victoria earthquake (magnitude 5.9, with an epicentre located 127 km from the Melbourne CBD) was selected to simulate seismic damage in buildings. To generate seismic excitations at the bedrock and soil surface, five soil blocks were created for the CLUE area, as shown in Figure 6. These blocks were developed by refining the soil map provided by McPherson & Hall (2007) with additional data from open-source borehole information and geotechnical reports (Golder, 2013; Golder, 2016; and AJM, 2018). In the refined soil map (Figure 6b), each soil block is represented by five unique borehole records.

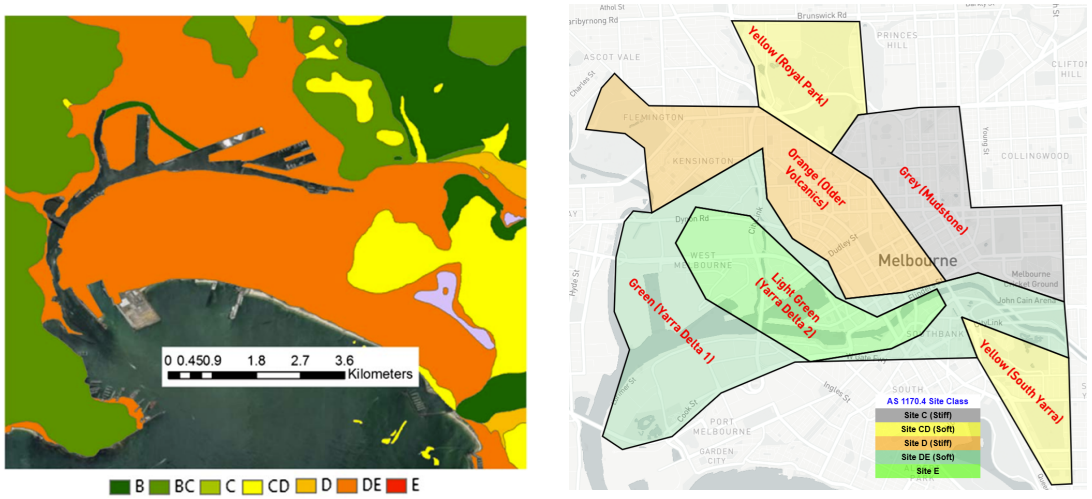

(a) Soil map of Melbourne (McPherson and Hall, 2007)

(b) Refined soil block map used in the virtual city assessment

Figure 6. Soil block map of CLUE area used into the soil amplification analysis.

The accelerogram recorded in Melbourne (station name: SRCHQ) (Hoult et al., 2021) was adjusted/scaled according to the methodology outlined in Section 2.1. An average decimal MMI value of 3.9, with a corresponding PGV(MMI) of 1.17 cm/s, was determined at a stiff site in Melbourne, located 127 km away from the source (as highlighted in Figure 7(a)). Additionally, a second stiff site, located 75 km away from the source with an MMI of 5 and a corresponding PGV(MMI) of 2.49 cm/s, was selected (as shown in Figure 7(b)). Next, the PGV(MMI) values from these two locations were used to calibrate the wave transmission quality factor Q_o, resulting in a calibrated value of 81. For Q_o = 190 and a PGV(MMI) of 1.17 cm/s, the optimised stress drop was calculated to be 136 bars. Finally, the original accelerogram was scaled using the mean target spectrum shown in Figure 8. The original and scaled bedrock accelerograms for the five soil blocks of the Clue Area in Melbourne are presented in Figure 9.

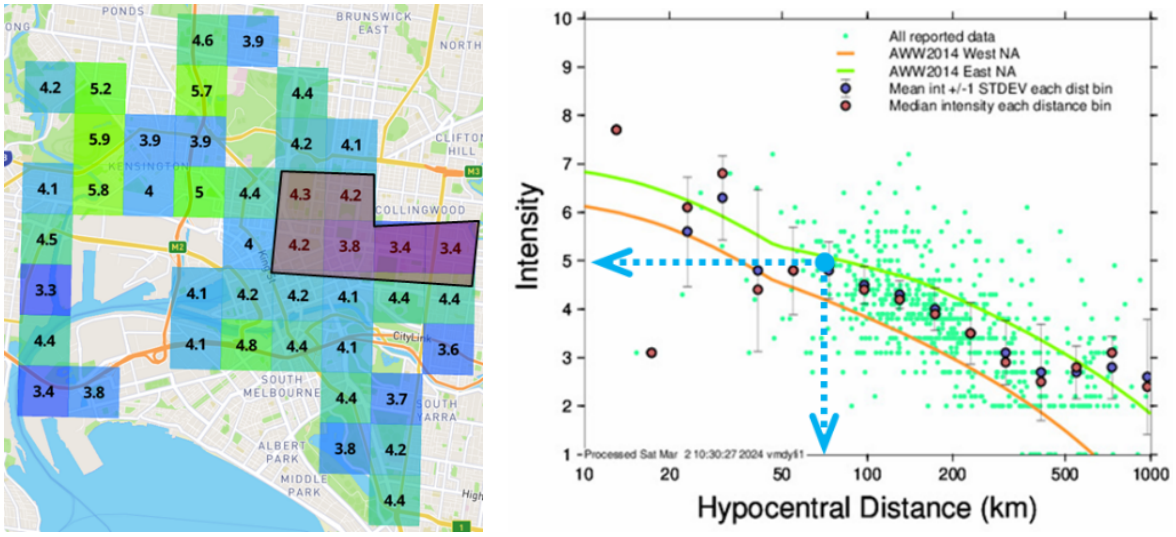

(a) MMI CLUE area

(b) MMI vs distance

Figure 7. Decimal MMI obtained from the USGS Felt report (USGS, 2021).

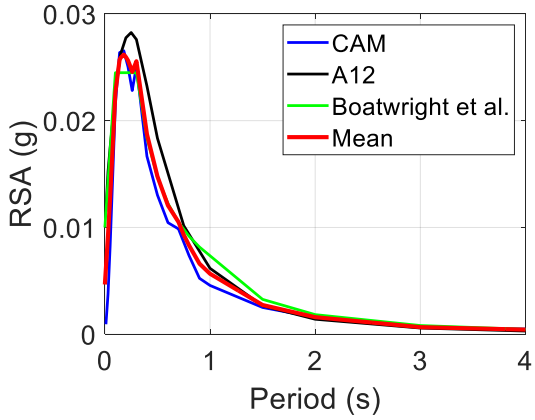

Figure 8. Mean target spectrum.

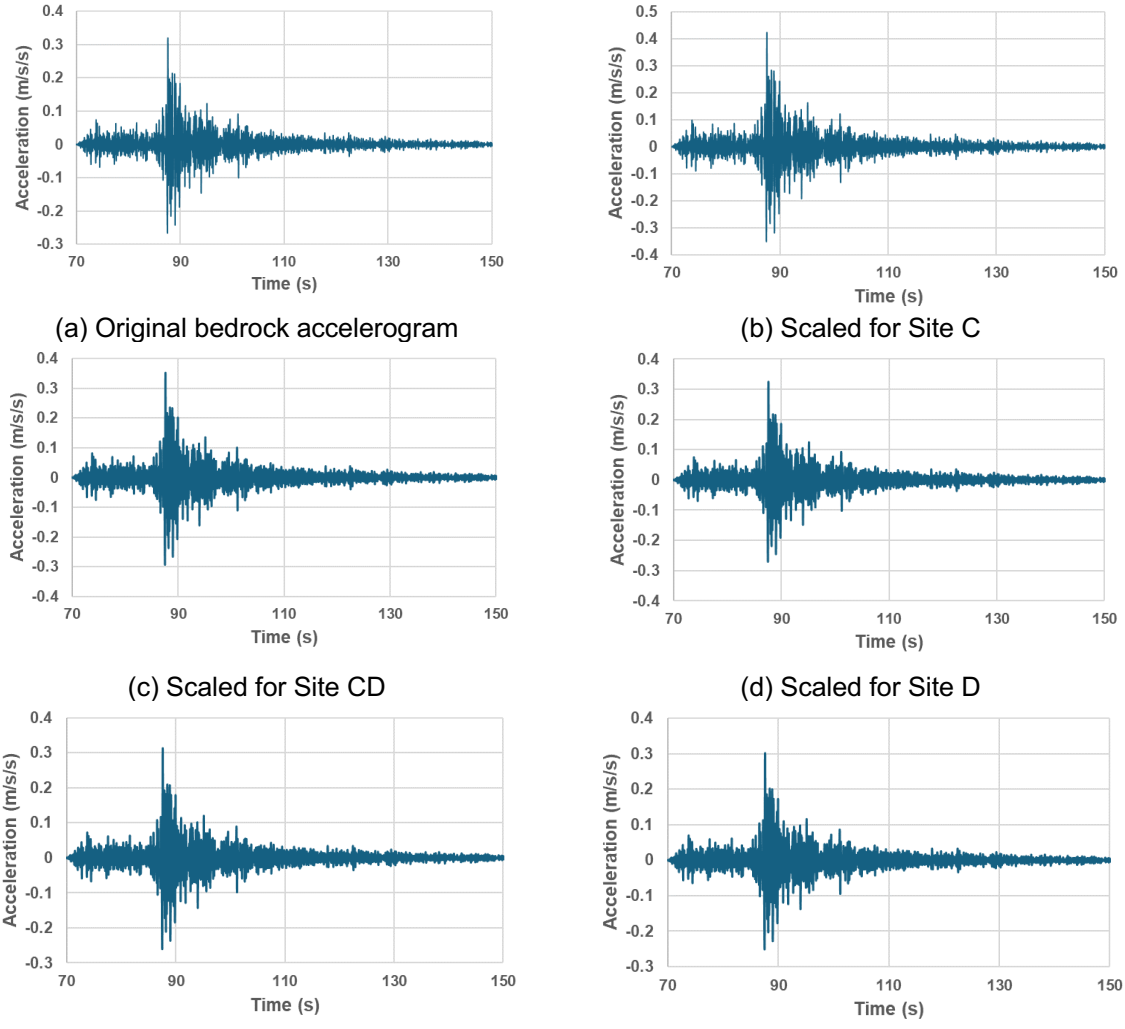

(a) Original bedrock accelerogram

(b) Scaled for Site C

(c) Scaled for Site CD

(d) Scaled for Site D

(e) Scaled for Site DE

(f) Scaled for Site E

Figure 9. Comparison of the original and the adjusted bedrock accelerogram of the 2021 Woods Point Earthquake.

After adjusting the bedrock accelerograms, a soil amplification analysis was performed to convert them into soil surface accelerograms. For each of the 25 boreholes, the soil surface accelerograms were generated and input into the Rapid Nonlinear Time History Analysis (RNLTHA) to predict maximum and mean damage scenarios, as shown in Figure 10. The macroscopic models required for RNLTHA were automatically generated using the structural information extracted for each building, as described above. For more detailed information on

each building, users can interact with the virtual city model (shown in Figure 10) by clicking on individual buildings. This interaction reveals the structural ID of the building, the drift level, and the expected damage level in each wall. Additionally, the model provides recommendations regarding whether the building is safe or unsafe for reoccupation and whether the building requires no repair, minor repairs, seismic retrofitting, or full reconstruction.

(a) Maximum prediction (b) Mean prediction

Figure 10. Virtual city showing the damage assessment results for the maximum and mean scenario.

The maximum damage assessment results shown in Figure 10(a) reveal that 13 out of 20 buildings had no damage, while 7 out of 20 buildings had slight damage. In contrast, the mean damage assessment results in Figure 10(b) show that 18 out of 20 buildings had no damage, and 2 out of 20 buildings had slight damage. In both scenarios, all buildings are considered safe for immediate reoccupation. The low level of damage predicted is attributed to the low level of ground shaking, as reflected by the MMI map in Figure 7.

4 Conclusions

The proposed rapid assessment methodology represents a significant advancement in the post-earthquake evaluation of reinforced concrete buildings. By integrating deep learning for footprint extraction, realistic earthquake excitation modelling, and advanced damage detection technologies, this approach provides a reliable and efficient means of assessing building safety immediately following an earthquake. The case study in Melbourne demonstrates the practical applicability and effectiveness of the method to reinforced concrete buildings, underscoring its potential to enhance rescue and recovery efforts. Future research will focus on refining this methodology and expanding its application to various building types across Australia. While the general approach remains consistent, the specific rules for detecting structural features will need adjustments for each building type. For assessments in seismic regions outside Australia, local Ground Motion Prediction Equations may replace the CAM model used in this study.

5 References

Abdollahi, A., Pradhan, B., Gite, S., & Alamri, A. (2020). Building footprint extraction from high resolution aerial images using generative adversarial network (GAN) architecture. *IEEE Access, 8*, 209517-209527. https://doi.org/10.1109/ACCESS.2020.3035567

American Society of Heating, Refrigerating and Air-Conditioning Engineers. (2023). *ASHRAE handbook—HVAC applications*. ASHRAE.

Aryal, J., & Neupane, B. (2023). Multi-scale feature map aggregation and supervised domain adaptation of fully convolutional networks for urban building footprint extraction. *Remote Sensing, 15*(2), 488. https://doi.org/10.3390/rs15020488

Atkinson, G. M., & Kaka, S. I. (2007). Relationships between felt intensity and instrumental ground motion in the central United States and California. *Bulletin of the Seismological Society of America, 97*(2), 497-510. https://doi.org/10.1785/0120060144

Bhatia, A. (2013). Stairwell Pressurization Systems. Continuing Education and Development.

Boatwright, J., Bundock, H., & Seekins, L. C. (2006). Using Modified Mercalli intensities to estimate acceleration response spectra for the 1906 San Francisco earthquake. Earthquake Spectra, 22(2_suppl), 279-295.

City of Melbourne. (2020). 2020 Building Footprints. https://data.melbourne.vic.gov.au/explore/dataset/2020-building-footprints/information/

Gao, W., Zhang, C., Lu, X., & Lu, W. (2023). Concrete spalling damage detection and seismic performance evaluation for RC shear walls via 3D reconstruction technique and numerical model updating. *Automation in Construction, 156*, 105146. https://doi.org/10.1016/j.autcon.2023.105146

Golder Associates. (2013). *Fishermans Bend precinct: High level geotechnical input* (Report No. 127613038-003-R-Rev0). Golder Associates. https://www.fishermansbend.vic.gov.au/__data/assets/pdf_file/0015/30381/16_Volume_3_High_Level_Geotechnical_Input.pdf

Golder Associates. (2016). *Interpreted geological setting EES summary report: Appendix C* (Report No. 1525532-218-R-Rev2). Golder Associates. https://bigbuild.vic.gov.au/__data/assets/pdf_file/0013/51115/MT-Technical-Appendix-P-Ground-Movement-and-Land-Stability-Part-5.pdf

Google LLC. (2024). *Google Earth* [Computer software]. https://www.google.com/earth

Hasan, M. I., & Yazdani, N. (2016). An experimental and numerical study on embedded rebar diameter in concrete using ground penetrating radar. *Chinese Journal of Engineering, 2016*(1), 9714381. https://doi.org/10.1155/2016/9714381

Hoult, R. D., Pascale, A., Jones, A., & Allen, T. (2021, November). The MW 5.9 Woods Point earthquake: A preliminary investigation of the ground motion observations. In *Proceedings of the Australian Earthquake Engineering Society 2021 Conference*, Virtual (pp. 25-26).

Hu, Y., Khatiwada, P., Tsang, H. H., & Menegon, S. (2023). Site-specific response spectra and accelerograms on bedrock and soil surface. *CivilEng, 4*(1), 311-332. https://doi.org/10.3390/civileng4010026

Hurley, M. J., Gottuk, D. T., Hall Jr, J. R., Harada, K., Kuligowski, E. D., Puchovsky, M., & WIECZOREK, C. J. (Eds.). (2015). *SFPE handbook of fire protection engineering*. Springer.

International Code Council. (Year). Fire and smoke protection features. In *International Building Code*. International Code Council.

Khatiwada, P., Hu, Y., Lam, N., & Menegon, S. J. (2023b). Nonlinear dynamic analyses utilizing macro-models of reinforced concrete building structures and site-specific accelerograms. *CivilEng, 4*(3), 881-900. https://doi.org/10.3390/civileng4030052

Khatiwada, P., Hu, Y., Lumantarna, E., & Menegon, S. J. (2023c). Dynamic modal analyses of building structures employing site-specific response spectra versus code response spectrum models. *CivilEng, 4*(1), 134-150. https://doi.org/10.3390/civileng4010013

Khatiwada, P., Lumantarna, E., & Lam, N. (2023a). Seismic vulnerability assessment of buildings at an urban scale.

Kokusho, T., & Sato, K. (2008). Surface-to-base amplification evaluated from KiK-net vertical array strong motion records. *Soil Dynamics and Earthquake Engineering, 28*(9), 707-716. https://doi.org/10.1016/j.soildyn.2008.01.008

Klote, J. H. (1988). An analysis of the influence of piston effect on elevator smoke control. Center for Fire Research, Berkeley, USA.

Laxman, K., Tabassum, N., Ai, L., Cole, C., & Ziehl, P. (2023). Automated crack detection and crack depth prediction for reinforced concrete structures using deep learning. *Construction and Building Materials, 370*, 130709. https://doi.org/10.1016/j.conbuildmat.2022.130709

Lee, T., & Kim, T. (2013). Automatic building height extraction by volumetric shadow analysis of monoscopic imagery. *International Journal of Remote Sensing, 34*(16), 5834-5850. https://doi.org/10.1080/01431161.2012.742153

Lou, Y., Meng, S., & Zhou, Y. (2024). Deep learning-based three-dimensional crack damage detection method using point clouds without color information. *Structural Health Monitoring*, 14759217241236929. https://doi.org/10.1177/14759217241236929

McPherson, A. A. (2007). Development of the Australian national regolith site classification map. Geoscience Australia.

Menegon, S. J. (2018). Displacement behaviour of reinforced concrete walls in regions of lower seismicity. Doctor of Philosophy thesis, Department of Civil and Construction Engineering, Swinburne University of Technology.

Nearmap. (2024). *Map of Melbourne*. https://www.nearmap.com

Pejic, T., & Allen, T. I. (2024). Crowd-sourced felt reports for 22 September 2021 MW 5.9 Woods Point earthquake: Actions of the public. *The Australian Journal of Emergency Management, 39*(2), 51-56. https://doi.org/10.47366/ajem.2024.0051

QGIS Development Team. (2024). *QGIS* [Computer software]. https://www.qgis.org

Shu, J., Zhang, C., Yu, K., Shooshtarian, M., & Liang, P. (2023). IFC-based semantic modeling of damaged RC beams using 3D point clouds. *Structural Concrete, 24*(1), 389-410. https://doi.org/10.1002/suco.202300011

Standards Australia. (2015). *AS 1668.1:2015 The use of ventilation and air conditioning in buildings, Part 1: Fire and smoke control in buildings*. Standards Australia.

Tang, Y., Lam, N., Tsang, H. H., & Lumantarna, E. (2019). Use of macroseismic intensity data to validate a regionally adjustable ground motion prediction model. *Geosciences*, *9*(10), 422.

Tang, Y., Lam, N. T., Tsang, H. H., & Lumantarna, E. (2022). An adaptive ground motion prediction equation for use in low-to-moderate seismicity regions. *Journal of Earthquake Engineering, 26*, 2567–2598. https://doi.org/10.1080/13632469.2021.2008720

Tsang, H. H., Wilson, J. L., Lam, N. T. K., & Su, R. K. L. (2017). A design spectrum model for flexible soil sites in regions of low-to-moderate seismicity. *Soil Dynamics and Earthquake Engineering, 92*, 36-45. https://doi.org/10.1016/j.soildyn.2016.11.017

U.S. Geological Survey. (Year). *M 5.9 - 39 km S of Mount Buller, Australia: Did you feel it?* https://earthquake.usgs.gov/earthquakes/eventpage/us7000fd9v/dyfi/intensity

Wald, D. J., Quitoriano, V., Dengler, L. A., & Dewey, J. W. (1999). Utilization of the Internet for rapid community intensity maps. *Seismological Research Letters, 70*(1), 68-80. https://doi.org/10.1785/gssrl.70.1.68

Wilkie, J., & Gibson, G. (1995). Estimation of seismic quality factor Q for Victoria, Australia. *AGSO Journal of Geology & Geophysics*, *15*(4), 511-517.

Wu, X., Wang, J., & Li, X. (2022). High-accuracy and efficient automatic building footprint extraction from high-resolution aerial images using convolutional neural networks. *Remote Sensing, 14*(8), 1958. https://doi.org/10.3390/rs14081958

Yang, T., & Li, X. (2021). Building footprint extraction from high-resolution imagery using a hybrid deep learning approach. *Remote Sensing, 13*(5), 851. https://doi.org/10.3390/rs13050851

Yao, M., & Liu, Z. (2024). 3D modeling of urban environments for building footprint extraction and visualization. *Computers, Environment and Urban Systems, 92*, 101-115. https://doi.org/10.1016/j.compenvurbsys.2023.101115

Zhang, M., Wu, Y., Li, Q., & Sun, X. (2023). High-resolution building footprint extraction using an end-to-end deep learning framework. *ISPRS Journal of Photogrammetry and Remote Sensing, 184*, 113-127. https://doi.org/10.1016/j.isprsjprs.2022.12.005

Zhu, X., Li, Y., & Wang, H. (2024). Generative adversarial network-based approach for building footprint extraction from satellite imagery. *Journal of Applied Remote Sensing, 18*(2), 045505. https://doi.org/10.1117/1.JRS.18.045505